Asynchronous Time Integration for Polynomial Chaos Expansion of Uncertain Periodic Dynamics

O.P. Le Maître[a,*], L. Mathelin[a], O.M. Knio[b], M.Y. Hussaini[c]

[a] *LIMSI-CNRS, 91403 Orsay cedex, France*
[b] *Department of Mechanical Engineering, Johns Hopkins University, Baltimore, MD 21218, USA*
[c] *Computational Science & Engineering – Department of Mathematics, Tallahassee, FL 32306-4510, USA*

Abstract

The simulation of dynamical systems involving random coefficients by means of stochastic spectral methods (Polynomial Chaos or other types of orthogonal stochastic expansions) is faced with well known computational difficulties, arising in particular due to the broadening of the solution spectrum as time evolves. The simulation of such systems thus requires increasing the basis dimension and computational resources for long time integration. This paper deals with systems having almost surely a stable limit cycles. It is proposed to reformulate the problem at hand in a rescaled time framework such that the spectrum of the rescaled solution remains narrow-banded. Two variants of this approach are considered and evaluated. The first relies on an explicit expression of a time-dependent, uncertain, time scale related to some distance between the corresponding solution and a reference deterministic system. The time scale is adjusted at each time step so that the distance from the reference system solution remains small, mimicking "in phase" behavior. The second variant achieves the same objective by borrowing concepts from optimal control theory, and yields more precise time-scale estimates at the price of a higher CPU cost. It is thus more appropriate for uncertain systems exhibiting a stiff behavior and complex limit cycles. The method is applied to the case of a linear oscillator with uncertain properties, and to a stiff nonlinear chemical system involving uncertain reaction constants. The tests demonstrate the effectiveness of the proposed approaches, at least in situations where the topology of the limit cycle does not change when the uncertain system parameters vary.

Key words: Dynamical systems, uncertainty, limit-cycle, Polynomial Chaos

1. Introduction

Deterministic physical systems can be studied by means of mathematical models designed to mimic their actual dynamics. These mathematical models can be constructed from physical considerations (for instance expressing elementary conservation principles) or from more heuristic considerations based on expertise. In both cases, the modeling process results in a fixed-form mathematical model involving parameters (or coefficients) that define the actual system of interest among the class of dynamics that the model can reproduce. Often, the parameter values are not explicitly known *a priori* and one relies on calibration or identification procedures to prescribe appropriate values to match, in some sense, a set of experimental observations for the actual system. Because such calibration procedures are usually inexact (due to measurement and model errors), the model parameters are generally subject to uncertainty, and assessing the impact on the model dynamics of the uncertainty on the parameters is crucial to gain confidence in the model predictions. This is classically achieved by means of (local) deterministic sensitivity analysis, such as adjoint techniques, or

* *Corresponding author*: LIMSI-CNRS, BP 133, F-91403 Orsay cedex, France.
Phone: (33)-1 69 85 80 76
Email addresses: olm@limsi.fr (O.P. Le Maître), mathelin@limsi.fr (L. Mathelin), knio@jhu.edu (O.M. Knio), myh@math.fsu.edu (M.Y. Hussaini)

Preprint November 2009 *December 4, 2009*

perturbation methods. In this paper, we follow an alternative, probabilistic approach where the uncertain model parameters are considered as random quantities with known probability laws.

One can basically distinguish between two main classes of methods for quantifying the impact of random parameters in a numerical model. The first includes simulation methods (such as Monte Carlo), which consist in evaluating the model solution point-wise in the parameter domain. These collocation approaches require only deterministic analysis tools and the dynamics of the random model is finally characterized from the collection (sample set) of model outputs corresponding to different parameter values. This makes the simulation methods both simple to implement using legacy codes, and numerically robust. However, solving the dynamics for a large collection of parameter values may represent a formidable task, requiring an overwhelming CPU effort. For instance, in the context of aeroelasticity, one has to solve a coupled fluid-structure problem and the large number of required simulations to achieve sufficiently converged statistics can make the use of this approach impractical.

An interesting alternative approach was initiated by the seminal works of Wiener [15] and Ghanem and Spanos [8] and relies on a spectral representation of the model solution dependence with regard to the uncertain parameters. The solution is now typically described in the random parameter space using stochastic polynomial series at the expense of solving a series of problems for the expansion coefficients of the solution. The expansion, or spectral, coefficients can be determined through collocative approaches, with the inherent advantages and limitations of such methods, or by means of a reformulation of the model equations, through the so-called stochastic Galerkin projection procedure, necessitating an additional development to adapt the deterministic codes. In the following we focus on the latter type of techniques, *i.e.*, the stochastic Galerkin methods for time-dependent problems.

Despite a rapidly developing literature on the subject, some issues concerning stochastic Galerkin methods for uncertainty quantification remain essentially unresolved. A well-known difficulty is the simulation of uncertain time-dependent problems over long times. Indeed, the uncertainty of model parameters usually affects the system phase velocity (assuming of course that such a phase may be unambiguously defined), and the complexity of the solution continuously increases with time as the system phase becomes more and more uncertain. This increasing complexity immediately translates in a broadening spectral content, precluding accurate approximations using usual discretization techniques based on fixed-order stochastic polynomial bases. This effect has been extensively studied by [11] and [13], who showed that a stochastic, polynomial-based representation, such as Polynomial Chaos, fails to represent the solution after a certain time.

In an effort to address this problem, [14] considered a multi-element generalized Polynomial Chaos approach. It essentially consists in approximating the random parameter dependence of the solution by piece-wise polynomials. However, this only postpones the time at which the approximation breaks down, namely by increasing the approximation accuracy using *hp*-refinement of the stochastic discretization. The refinement also implies an increasing number of terms in the expansion of the solution, and consequently leads to a high solution cost. A similar idea was pursued by [13] who employed a wavelet-based Multi-Resolution Analysis in the context of time-dependent problems with uncertain parameters. They studied a nonlinear aeroelastic computational model involving uncertain parameters and found that stochastic representations using Wiener-Haar wavelets [9] lead to a good representation of the solution until large times. However, this approach still suffers from the same drawback facing the multi-element approach, in the sense that the breakdown of the approximation is delayed but not remedied.

An interesting class of problems where the aforementioned difficulties above also arise corresponds to situations where the dynamics of the system possess almost surely an asymptotic, stable, limit cycle (LC) which may depend on the uncertain parameters. In this context, several specific techniques have been proposed to access a probabilistic description of the uncertain limit cycle. [18] makes use of an equation-free technique to study the limit-cycle of a random chemical system, whereas [2] investigates the limit-cycle oscillations for an airfoil under uncertainty using Polynomial Chaos. However, the above methods are either limited in scope, namely being applicable to the limit cycle only, or limited to small times, specifically time intervals that are not large enough that a low or moderate order approximation ceases to be adequate due to the broadening spectrum of the stochastic solution. A somewhat more general approach was followed in [16] and [17], where different, well chosen, realizations of the uncertain system were approximated in the

stochastic space at constant phase. This approach relies on the expression of the time-dependent random quantity of interest as a time-independent random variable function of some phase. The solution dependence on the stochastic parameters is approximated using stochastic polynomials and the solution may be expressed in time using an inverse transformation relating phase and time. The methodology has been applied to the Duffing oscillator, and to an elastically mounted airfoil with uncertain natural frequencies.

The present work was developed independently from that of [16] and [17], but relies on some conceptually similar grounds. The core idea is to reformulate the problem so that the dynamics depend on a rescaled time. To this end, an uncertain time scale is introduced which acts as a "local" clock in the stochastic parameter domain. This time scale is adjusted so as to maintain the uncertain dynamics "in phase" as much as possible. This is achieved by introducing additional equations for the dynamics of the uncertain time scale.

To describe the present approach, we first discuss in section 2 some preliminary tools that are useful in the uncertainty quantification context. In section 3, we discuss in detail a first implementation based on a linear adjustment of the local "clock." The effectiveness of this implementation is demonstrated in section 4 for the case of a simple linear oscillator with uncertain frequency. A second, more general, implementation of the present approach is then developed in section 5, where an adjoint-based control problem is used to determine the uncertain time scale minimizing optimally the increase in phase uncertainty as time elapses. This strategy is successfully applied in section 6 for the time integration of a non linear chemical system having uncertain rate parameters. Major conclusions are drawn in section 7.

2. Dynamical systems with uncertain coefficients

2.1. Uncertain system

Let us consider a dynamical system described by its state vector $\boldsymbol{x} \in \mathbb{R}^n$. We assume that the system is autonomous, and that it is governed by a set of n ODEs of the form:

$$\frac{d\boldsymbol{x}}{dt} = \boldsymbol{f}(\boldsymbol{x}; q), \tag{1}$$

with initial conditions at time $t = 0$ given by:

$$\boldsymbol{x}(t = 0) = \boldsymbol{x}^0. \tag{2}$$

For simplicity, we shall assume that the initial conditions are certain. In the expression of f in (1), q is a vector of coefficients specifying the dynamics. The coefficients (or a subset of) q are assumed uncertain and are considered as random, with known probability law defined on an abstract probability space $\mathcal{P} = (\Omega, \Sigma, \mathrm{d}P)$, where Ω denotes the set of random events, Σ is the σ-algebra of the events, and P is the probability measure. By $q(\omega \in \Omega)$ we shall denote a realization of the system coefficients. Since the dynamics of the system depend on the coefficients q, the solution $\boldsymbol{x}(t > 0)$ is random, defined on $\mathcal{P}$, and $\boldsymbol{x}(t, \omega)$ is the realization of the system corresponding to $q(\omega)$. We further denote by $L_2(\Omega, \Sigma, \mathrm{d}P)$, or simply $L_2(\Omega)$, the space of second order random variables defined on $\mathcal{P}$. The space $L_2(\Omega)$ is equipped with the inner product $\langle , \rangle$,

$$\langle u, v \rangle = E\left[uv\right], \quad \forall u, v \in L_2 \tag{3}$$

and associated norm $\|u\|_\Omega \equiv \langle u, u \rangle^{1/2}$. Here, $E[.]$ is the expectation operator defined according to:

$$E[f] \equiv \int_\Omega f(\omega) \mathrm{d}P(\omega). \tag{4}$$

We thus have:

$$u \in L_2(\Omega) \Longleftrightarrow E\left[u^2\right] = \int_\Omega u^2(\omega) \mathrm{d}P(\omega) < \infty. \tag{5}$$

2.2. Parametric uncertainty

For the solution of (1), we need to perform a stochastic discretization. To this end, we introduce a set of N random variables $\boldsymbol{\xi} \equiv \{\xi_1, \dots, \xi_\mathrm{N}\}$, defined on $\mathcal{P}$, with known density $p_{\boldsymbol{\xi}}$. For simplicity, we restrict ourselves here to the case of independent identically distributed random variables, so p_ξ admits the factorized form:

$$p_{\boldsymbol{\xi}}(\boldsymbol{\xi}) = \prod_{i=1}^{\mathrm{N}} p(\xi_i). \tag{6}$$

In addition, let $\Xi \in \mathbb{R}^\mathrm{N}$ be the range of $\boldsymbol{\xi}$ and define $\mathcal{P}_\Xi = (\Xi, \mathcal{B}_\Xi, p_{\boldsymbol{\xi}})$ the so-called image probability space, where $\mathcal{B}_\Xi$ is the Borel set of Ξ. By $L_2(\Xi)$ we will denote the space of random variables $u(\boldsymbol{\xi})$ with finite second moment, i.e.

$$u(\boldsymbol{\xi}) \in L_2(\Xi) \Longleftrightarrow E[u^2(\boldsymbol{\xi})] = \int_\Omega u^2(\boldsymbol{\xi}(\omega)) \mathrm{d}P(\omega) = \int_\Xi u^2(\boldsymbol{\xi}) p_{\boldsymbol{\xi}}(\boldsymbol{\xi}) \mathrm{d}\boldsymbol{\xi} \equiv \left\langle u^2 \right\rangle < \infty. \tag{7}$$

In the following, we will use the bracket $\langle \cdot \rangle$ to indicate the expectation evaluated in the image space.

The random variables $\xi_1, \dots, \xi_\mathrm{N}$ are used to parameterize the uncertain parameters in (1), such that

$$q(\omega) \equiv q(\boldsymbol{\xi}(\omega)), \tag{8}$$

and the solution can be simply expressed as $\boldsymbol{x}(t; \boldsymbol{\xi})$. In the following, we shall restrict ourselves to systems having stable limit cycles (LC) in the state space, *i.e.*, $\boldsymbol{x}(t; \boldsymbol{\xi})$ almost surely converges to a periodic solution as $t \to \infty$. The objective is then to compute the stochastic LC of the dynamics, and to compute statistical quantities of interest, such as the distributions of the system frequency and of the amplitudes of the trajectory.

2.3. Stochastic spectral expansion

Introducing a complete orthonormal set (CONS) $\{\Psi_0, \Psi_1, \cdots\}$ of functionals in $\boldsymbol{\xi}$ spanning $L_2(\Xi)$, and assuming that $\boldsymbol{x}(t; \boldsymbol{\xi}) \in L_2(\Xi)$ for all $t \geq 0$ (*i.e.*, that each of the components of $\boldsymbol{x}$ are in $L_2(\Xi)$), the state of the system can be expanded in a Fourier-like series of the form:

$$\boldsymbol{x}(t; \boldsymbol{\xi}) = \sum_{k=0}^{\infty} \boldsymbol{x}_k(t) \Psi_k(\boldsymbol{\xi}), \tag{9}$$

where $\boldsymbol{x}_k \in \mathbb{R}^n$ are (deterministic) expansion coefficients. Using the orthonormality property of the CONS,

$$\langle \Psi_k(\boldsymbol{\xi}) \Psi_l(\boldsymbol{\xi}) \rangle = \delta_{kl} \quad \forall k, l \geq 0, \tag{10}$$

the expansions coefficients can be expressed as

$$\boldsymbol{x}_k(t) = \langle \boldsymbol{x}(t; \boldsymbol{\xi}) \Psi(\boldsymbol{\xi}) \rangle \,. \tag{11}$$

A classical choice for the Ψ_k are polynomials, in which case (9) corresponds to the Polynomial Chaos (PC) expansion. For random variables having reduced centered normal distributions, $\xi_{i=1,\dots,\mathrm{N}} \sim \mathcal{N}(0, 1)$, the Ψ_k are generalized Hermite polynomials; see Wiener [15] and Cameron and Martin [3]. PC expansions with other types of distributions for the ξ_i were proposed in [19], while expansions in terms of piecewise polynomial functionals or multiwavelets were considered in [4, 9, 10, 14]. The results below immediately extend to any type of orthonormal expansions, although we shall only consider polynomial bases.

3. Asynchronous time integration

3.1. Time scaling

We introduce a transformed time variable, τ, which we allow to depend on the random variables $\boldsymbol{\xi}$ parameterizing the dynamics. We shall refer to $\tau(t;\boldsymbol{\xi})$ as the locally rescaled time, and specify in terms of the mapping:

$$\tau \ : [0,\infty) \times \Xi \mapsto \tau(t;\boldsymbol{\xi}) \in \mathbb{R}^+ \times L_2(\Xi). \tag{12}$$

We further constrain τ such that

$$\frac{d\tau}{dt} \equiv \dot{\tau}(t;\boldsymbol{\xi}) > 0 \quad \forall t > 0, \forall \boldsymbol{\xi} \in \Xi. \tag{13}$$

Consequently, τ is an almost surely increasing function of t and, given $\boldsymbol{\xi}(\omega)$, there is an univocal relation between t and $\tau(\cdot;\boldsymbol{\xi}(\omega))$. This property allows us to define unambiguously a new (transformed) stochastic process $\boldsymbol{y}$ such that

$$\boldsymbol{y}(t;\boldsymbol{\xi}) = \boldsymbol{x}(\tau(t;\boldsymbol{\xi});\boldsymbol{\xi}) \quad a.s. \tag{14}$$

In the following, $\dot{\tau}$ will be referred to as the clock speed. The governing equations for $\boldsymbol{y}$ are easily derived using chain-rule differentiation; we obtain:

$$\frac{d\boldsymbol{y}}{dt} = \frac{d\boldsymbol{x}}{d\tau}\frac{d\tau}{dt} = \dot{\tau}(t;\boldsymbol{\xi})\boldsymbol{f}(\boldsymbol{y}(t;\boldsymbol{\xi});q(\boldsymbol{\xi})). \tag{15}$$

3.2. Reference dynamics

The main idea underlying the proposed method is to construct the time scaling, $\tau(t;\boldsymbol{\xi})$, such that the uncertain trajectories of the system governed by (15) remain essentially "in phase" as t increases, *i.e.*, realizations $\boldsymbol{y}(t;\boldsymbol{\xi}(\omega))$ are clustered in a finite neighborhood of the state space. To this end, we introduce a reference trajectory $\boldsymbol{x}^r(t)$ of the system, governed by the **deterministic** system of ODEs:

$$\dot{\boldsymbol{x}^r} \equiv \frac{d\boldsymbol{x}^r}{dt} = \boldsymbol{f}^r(\boldsymbol{x}^r) = \boldsymbol{f}(\boldsymbol{x}^r;\overline{q}). \tag{16}$$

In (16), $\overline{q}$ is a prescribed realization of the parameters, selected such that $\boldsymbol{x}^r$ exhibits dynamics that are characteristic of the uncertain system. A convenient choice is to take $\overline{q}$ as the expectation of $q(\boldsymbol{\xi})$, *i.e.*

$$\overline{q} = \langle q(\boldsymbol{\xi})\rangle = \int_{\Xi} q(\boldsymbol{\xi}) p_{\boldsymbol{\xi}}(\boldsymbol{\xi}) d\boldsymbol{\xi}. \tag{17}$$

For $\boldsymbol{x}^r$ to be characteristic of the uncertain dynamics, it is necessary that the variability of the random coefficients does not induce qualitatively significant changes in the resulting limit cycle. In particular, it is assumed that there is no parametric bifurcation of the system dynamics in the uncertainty range. In other words, a smooth dependence of the system's LC with regards to the random parameters is assumed.

Remark 1. *Note that whenever the assumption on the smooth dependence of the LC on the random coefficients does not hold, one can generally seek a partition of the random parameter space so as to construct decoupled problems for which the assumption is independently (or locally) satisfied.*

3.3. Definition of the time transformation

We wish to construct the time rescaling $\tau(t;\boldsymbol{\xi})$ so that all realizations of the dynamics remain in a small neighborhood of reference trajectory $\boldsymbol{x}^r(t)$. Thus, we want to minimize in some sense the distance between $\boldsymbol{y}(t;\boldsymbol{\xi})$ and $\boldsymbol{x}^r(t)$. For a (small) time increment δt, the Taylor expansion of $\boldsymbol{y}$ about t is

$$\begin{aligned} \boldsymbol{y}(t+\delta t;\boldsymbol{\xi}) &= \boldsymbol{y}(t;\boldsymbol{\xi}) + \delta t\, \dot{\tau}(t;\boldsymbol{\xi})\boldsymbol{f}(\boldsymbol{y}(t;\boldsymbol{\xi});q(\boldsymbol{\xi})) \\ &+ \frac{\delta t^2}{2}\left[\, \boldsymbol{f}(\boldsymbol{y}(t;\boldsymbol{\xi});q(\boldsymbol{\xi}))\, \ddot{\tau}(t;\boldsymbol{\xi})\right. \end{aligned}$$

$$+ \quad \dot\tau^2(t;\boldsymbol{\xi})\,\boldsymbol{\nabla f}(\boldsymbol{y}(t;\boldsymbol{\xi});q(\boldsymbol{\xi}))\,\boldsymbol{f}(\boldsymbol{y}(t;\boldsymbol{\xi});q(\boldsymbol{\xi}))\,\big] + \mathcal{O}(\delta t^3), \tag{18}$$

where $\boldsymbol{\nabla f}$ is the Jacobian matrix of $\boldsymbol{f}$. Similarly, the Taylor expansion of $\boldsymbol{x}^r$ is

$$\boldsymbol{x}^r(t+\delta t) \;=\; \boldsymbol{x}^r(t) + \delta t \boldsymbol{f}^r(\boldsymbol{x}^r(t)) + \frac{\delta t^2}{2}\left[\boldsymbol{\nabla f}^r(\boldsymbol{x}^r(t))\boldsymbol{f}^r(\boldsymbol{x}^r(t))\right] + \mathcal{O}(\delta t^3). \tag{19}$$

Then, dropping the dependence on $\boldsymbol{\xi}$ to simplify the notation, we have

$$\begin{aligned}(\boldsymbol{y}-\boldsymbol{x}^r)(t+\delta t) \;&\approx\; (\boldsymbol{y}-\boldsymbol{x}^r)(t) + \delta t\left[\tau \boldsymbol{f}(\boldsymbol{y};q) - \boldsymbol{f}^r(\boldsymbol{x}^r)\right] \\ &+\; \frac{\delta t^2}{2}\left[\dot\tau^2 \boldsymbol{\nabla f}(\boldsymbol{y};q)\boldsymbol{f}(\boldsymbol{y};q) - \boldsymbol{\nabla f}^r(\boldsymbol{x}^r)\boldsymbol{f}^r(\boldsymbol{x}^r) + \ddot\tau \boldsymbol{f}(\boldsymbol{y};q)\right].\end{aligned} \tag{20}$$

Setting $d^2(t;\boldsymbol{\xi}) = \|\boldsymbol{y}(t;\boldsymbol{\xi}) - \boldsymbol{x}^r(t)\|^2$, where $\|\cdot\|$ is the usual Euclidean norm, we now want to minimize $d^2(t+\delta t;\boldsymbol{\xi})$ with regards to $\ddot\tau$. Using the approximates of $\boldsymbol{y}$ and $\boldsymbol{x}^r$ at time $t+\delta t$, the minimization of d^2 leads to:

$$\begin{aligned}\ddot\tau = \frac{1}{\|\boldsymbol{f}(\boldsymbol{y})\|^2}\Bigg[&-2\frac{\boldsymbol{y}-\boldsymbol{x}^r}{\delta t^2} - 2\frac{\dot\tau \boldsymbol{f}(\boldsymbol{y}) - \boldsymbol{f}^r(\boldsymbol{x}^r)}{\delta t} \\ &- \dot\tau^2 \boldsymbol{\nabla f}(\boldsymbol{y})\boldsymbol{f}(\boldsymbol{y}) + \boldsymbol{\nabla f}^r(\boldsymbol{x}^r)\boldsymbol{f}^r(\boldsymbol{x}^r)\Big]\cdot \boldsymbol{f}(\boldsymbol{y}).\end{aligned} \tag{21}$$

Remark 2. *The equation above provides us with an expression for the time derivative of the clock speed $\dot\tau(t,\boldsymbol{\xi})$. However this expression is difficult to exploit in its current form, mainly because of the non-linearities involved that prevent immediate implementation. Instead, letting $\delta t \to 0$, we observe that the leading term gives us*

$$\ddot\tau(t,\boldsymbol{\xi}) \sim \boldsymbol{f}(\boldsymbol{y}(t;\boldsymbol{\xi});q(\boldsymbol{\xi}))\cdot(\boldsymbol{y}(t;\boldsymbol{\xi}) - \boldsymbol{x}^r(t))\,. \tag{22}$$

This leads us to a consider a much simpler construction for the time transformation, directly amenable to numerical implementation. This first method is now introduced, on the basis of more heuristic considerations.

3.4. First method

In the state space, the shift between the reference and stochastic states is defined as

$$\boldsymbol{d}(t;\boldsymbol{\xi}) \equiv \boldsymbol{y}(t;\boldsymbol{\xi}) - \boldsymbol{x}^r(t). \tag{23}$$

From the assumption that the uncertainty qualitatively preserves the structure of the dynamics, *i.e.*, it yields smooth dependence of the state on $\boldsymbol{\xi}$, one can assume that trajectories for different realizations $\boldsymbol{\xi}(\omega)$ remain essentially parallel. At time t, an indicator of the direction tangent to the trajectories is $\boldsymbol{f}^r(\boldsymbol{x}^r(t))$. Consequently, two trajectories will be said to be "in-phase" if the shift $\boldsymbol{d}$ is perpendicular to the direction tangent to the reference trajectory. Accordingly, we want to re-scale time, for each realization of the system, such that trajectories are in-phase as much as possible, or in other words are contained in the plane normal to $\boldsymbol{f}^r$ at $\boldsymbol{x}^r$. Defining

$$\Delta(t;\boldsymbol{\xi}) \equiv \boldsymbol{d}(t;\boldsymbol{\xi})\cdot\boldsymbol{f}^r(\boldsymbol{x}^r(t)), \tag{24}$$

the "in-phase" constraint reads $\Delta(t,\boldsymbol{\xi}) = 0$. In attempting to satisfy this constraint, we are lead to the following simple rules: if $\Delta(t;\boldsymbol{\xi}(\omega)) < 0$ the local clock speed $\dot\tau(t;\boldsymbol{\xi}(\omega))$ has to be increased for the corresponding realization to catch up with the reference, whereas conversely if $\Delta(t;\boldsymbol{\xi}(\omega)) > 0$ the clock speed $\dot\tau(t;\boldsymbol{\xi}(\omega))$ has to be slowed down. We also observe that in fact $\Delta(t;\boldsymbol{\xi})$ corresponds to the right-hand side of (22), where $\boldsymbol{f}$ has been substituted with the reference $\boldsymbol{f}^r$.

There are many different ways to implement the previous rules; a convenient way is to simply adjust the clock speed according to:

$$\frac{d\dot\tau}{dt} = -\alpha_0\dot\tau(t;\boldsymbol{\xi})\Delta(t;\boldsymbol{\xi}) + \alpha_1\left[1 - \dot\tau(t;\boldsymbol{\xi})\right]. \tag{25}$$

On the right-hand side of (25), the first terms updates the local clock according to the previous rules, whereas the second terms is introduced to ensure that the clock speed remains (on average) close to 1 and

the dynamics follows the reference. The constants α_0 and α_1 are both positive and need be properly selected to control the strength of the in-phase constraint enforcement and the stability of the local clock speed. We are thus left with the resolution of the following set of ODEs:

$$\begin{aligned}
\frac{d\boldsymbol{x}^r}{dt}(t) &= \boldsymbol{f}^r(\boldsymbol{x}^r(t)), && (26)\\
\frac{d\boldsymbol{y}}{dt}(t;\boldsymbol{\xi}) &= \dot{\tau}(t;\boldsymbol{\xi})\boldsymbol{f}(\boldsymbol{y}(t;\boldsymbol{\xi});q(\boldsymbol{\xi})), && (27)\\
\frac{d\dot{\tau}}{dt}(t;\boldsymbol{\xi}) &= -\alpha_0\dot{\tau}(t;\boldsymbol{\xi})\Delta(t;\boldsymbol{\xi}) + \alpha_1\left[1-\dot{\tau}(t;\boldsymbol{\xi})\right], && (28)\\
\frac{d\tau}{dt}(t;\boldsymbol{\xi}) &= \dot{\tau}(t;\boldsymbol{\xi}), && (29)
\end{aligned}$$

with initial conditions:

$$\begin{aligned}
\boldsymbol{x}^r(t=0) &= \boldsymbol{x}^0, && (30)\\
\boldsymbol{y}(t=0;\boldsymbol{\xi}) &= \boldsymbol{x}^0, && (31)\\
\dot{\tau}(t=0;\boldsymbol{\xi}) &= 1, && (32)\\
\tau(0;\boldsymbol{\xi}) &= 0. && (33)
\end{aligned}$$

Remark 3. *The updating of the local clock speed through (25) is primarily conceived for the purpose of illustrating the essential concepts behind controlling the rescaled time. In section 5 we shall derive more elaborate and robust strategies to achieve this goal. In particular, we emphasize that the stochastic differential approach proposed here does not necessarily guarantee that τ time is almost surely an increasing function of t.*

3.5. Stochastic Galerkin Projection

The governing system outlined above involves a deterministic evolution equation for the reference dynamics that is decoupled from a sub-system of coupled stochastic ODEs for $\boldsymbol{y}$, $\dot{\tau}$ and τ. Only the stochastic sub-system involves solutions dependent on $\boldsymbol{\xi}$ and so requires an appropriate treatment, whereas the reference dynamics can be integrated using standard techniques for ODEs.

To solve the stochastic ODEs for the uncertain quantities we rely on a classical stochastic Galerkin projection method, using PC expansions of the unknown quantities. The dependence of $\boldsymbol{y}$, $\dot{\tau}$ and τ on $\boldsymbol{\xi}$ is expressed in terms of truncated spectral expansions:

$$\left[\boldsymbol{y},\dot{\tau},\tau\right](t;\boldsymbol{\xi}) = \sum_{k=0}^{\mathrm{P}}\left[\boldsymbol{y},\dot{\tau},\tau\right]_k(t)\Psi_k(\boldsymbol{\xi}), \tag{34}$$

where, as discussed above, the Ψ_k are orthonormal polynomials in $\boldsymbol{\xi}$. The number of terms P in the expansion depends on the polynomial truncation order No, and is given by $\mathrm{P}+1 = (\mathrm{NNo})!/(\mathrm{N}!\mathrm{No}!)$. The Galerkin projection of the stochastic ODEs onto the polynomial basis results in:

$$\left\{\begin{array}{l}
\dfrac{d\boldsymbol{y}_k}{dt} = \left\langle \boldsymbol{f}\left(\displaystyle\sum_l \boldsymbol{y}_l\Psi_l;q(\boldsymbol{\xi})\right),\Psi_k\right\rangle,\\
\dfrac{d\dot{\tau}_k}{dt} = -\alpha_0\left\langle\left(\displaystyle\sum_l\dot{\tau}_l\Psi_l\right)\Delta(t;\boldsymbol{\xi}),\Psi_k\right\rangle + \alpha_1\left\langle\left(1-\displaystyle\sum_l\dot{\tau}_l\Psi_l\right)\Psi_k\right\rangle,\\
\dfrac{d\tau_k}{dt} = \dot{\tau}_k,
\end{array}\right. \tag{35}$$

for $k=0,\ldots,\mathrm{P}$. A Galerkin projection of the initial conditions is also used to determine the initial condition for each PC modes. The initial conditions being deterministic, and using the convention $\Psi_0 = 1$ *i.e.*, mode 0 is the mean mode, we have:

$$\boldsymbol{y}_0(t=0) = \boldsymbol{x}^0, \quad \dot{\tau}_0(t=0) = 1, \quad \tau_0(t=0) = 0, \tag{36}$$

and

$$\boldsymbol{y}_k(t=0)=0, \quad \dot{\tau}_k(t=0)=0, \quad \tau_k(t=0)=0, \quad k\geq 1. \tag{37}$$

In the computations below, the reference system and equations for the PC modes of $\boldsymbol{y}$, $\dot{\tau}$ and τ are time-integrated using a 4-th order Runge-Kutta scheme with a constant time step, Δt. The selection of an explicit time integration scheme avoids the need to solve non-linear equations, which would be the case with an implicit integrator. Nonetheless, we are still required to estimate the Galerkin projection of nonlinear terms, as for instance $\boldsymbol{f}(\boldsymbol{y};q(\boldsymbol{\xi}))$, $\dot{\tau}\Delta$. These projections are performed by means of pseudo-spectral techniques (see [5]).

Remark 4. *It is seen that the overall computational load consists in the integration of one deterministic system, and a coupled set of* $(n+2)(\mathrm{P}+1)$ *equations. Compared to the usual Galerkin projection, which amounts to the integration of a set of* $n(\mathrm{P}+1)$ *equations only, the proposed method may appear to require larger overhead arising from the time integration of the stochastic clock,* τ*, and clock speed,* $\dot{\tau}$*. However, this is not necessarily the case, because the proposed method actually allows the use of significantly lower expansion orders* No*. Consequently, the resulting CPU cost is effectively much lower for the asynchronous integration, because the classical Galerkin projection would require a much larger (and increasing) expansion order* No *to obtain the solution over long time intervals.*

4. Application to the linear oscillator

As an example of the procedure outlined in the previous section, we consider the simplest case of an undamped linear oscillator with random frequency. Specifically, we focus on the following equation of motion:

$$\frac{d\boldsymbol{x}}{dt}=[A]\boldsymbol{x}, \tag{38}$$

where $\boldsymbol{x}=(x\,\dot{x})^T\in\mathbb{R}^2$ is the state vector, with components corresponding to the position (x) and impulse ($\dot{x}$). The system matrix $[A]\in\mathbb{R}^{2\times 2}$ is of the form

$$[A]=\begin{pmatrix} 0 & 1 \\ -q & 0 \end{pmatrix}, \tag{39}$$

where $q>0$ is uncertain. The frequency of the system is $\sqrt{q}/2\pi$. The uncertain coefficient q is modeled as a random variable with uniform distribution over the interval $q_0\pm q_1$, with $0\leq q_1<q_0$. The coefficient q can be immediately parameterized using a single random variable ξ uniformly distributed on $[-1,1]$, namely according to:

$$q(\xi)=q_0+q_1\xi, \quad \xi\sim U[-1,1]. \tag{40}$$

Finally, we set the initial condition to $\boldsymbol{x}(t=0)=(1\,0)^T$, so the exact solution is

$$x(t;\xi)=\cos\left(\sqrt{q(\xi)}t\right), \quad \dot{x}(t;\xi)=-\sqrt{q(\xi)}\sin\left(\sqrt{q(\xi)}t\right). \tag{41}$$

The stochastic expansion basis therefore consists of the one-dimensional (normalized) Legendre polynomials [1].

4.1. Classical Galerkin Projection

Truncating the polynomial chaos expansion to order $\mathrm{No}>0$, the approximate solution can be expressed as:

$$\boldsymbol{x}(t;\xi)=\sum_{k=0}^{\mathrm{P=No}}\boldsymbol{x}_k(t)\Psi_k(\xi). \tag{42}$$

Applying the classical stochastic Galerkin procedure to (38), and using the orthonormality of the basis functions Ψ_k, one obtains the following set of coupled ODEs for the stochastic modes $\boldsymbol{x}_k(t)$:

$$\frac{d\boldsymbol{x}_k}{dt} = [A]_0\boldsymbol{x}_k + \sum_{l=0}^{\mathrm{P}} \langle \xi\Psi_l\Psi_k\rangle [A]_1\boldsymbol{x}_l, \quad \text{for } k = 0, 1, \ldots, \mathrm{P}, \tag{43}$$

where the two matrices $[A]_0$ and $[A]_1$ are respectively given by

$$[A]_0 = \begin{pmatrix} 0 & 1 \\ -q_0 & 0 \end{pmatrix}, \quad [A]_1 = \begin{pmatrix} 0 & 0 \\ -q_1 & 0 \end{pmatrix}. \tag{44}$$

The initial conditions for this set of ODEs are

$$\boldsymbol{x}_0(t=0) = \begin{pmatrix} 1 \\ 0 \end{pmatrix}, \boldsymbol{x}_{k>0}(t=0) = \begin{pmatrix} 0 \\ 0 \end{pmatrix}. \tag{45}$$

We set $q_0 = (2\pi)^2$ and $q_1 = 0.2q_0$. The time integration uses a 4th order RK scheme with small time step $\Delta t = 0.001$, such that the integration is essentially error-free.

Figure 1 shows solutions obtained for the classical Galerkin projection with No = 5 and No = 15. Plotted are the trajectories of the truncated solution in the state space, and the time evolution of the impulse $\dot{x}(t;\xi)$ with time, for different realizations of the coefficient $q(\xi)$ corresponding to $\xi(\omega) = \pm 1$, $\pm 1/2$ and 0, and for $t \in [0, 50]$. For both orders, we observe that the trajectories of the truncated solutions do not remain on exact limit cycles (also shown), but experience large deviations and complex a periodic dynamics. The evolutions of the realizations $\dot{x}(t;\xi(\omega))$ further inform us that by increasing the expansion order from No = 5 to No = 15 one obtains an accurate approximation of the dynamics over a longer time span: for No = 5 the trajectories significantly depart from the exact solution after $t \approx 5$ while for No = 15 the solution is correctly captured up to $t \approx 20$. However, the results illustrate that even for this simple system, an overly large expansion order is needed to obtain the correct dynamics over arbitrarily large time periods, and that the classical Galerkin approach is not feasible for long time integration. Evidently, for the present example this is not a real limitation since the system lies on its limit cycle at the initial time, such that it can be entirely characterized in just one period. However, for other systems exhibiting a slow convergence toward their asymptotic stable limit cycle, the issue of truncation error over long integration times makes the straightforward Galerkin projection essentially impractical.

4.2. Asynchronous time integration

We now consider simulating the stochastic system using the rescaled time approach, *i.e.*, we solve (35) for $\boldsymbol{y}(t;\xi)$, $\boldsymbol{x}^r(t)$, $\tau(t;\xi)$, and $\dot{\tau}(t;\xi)$, with initial condition $\boldsymbol{x}^r(t=0) = \boldsymbol{y}(t=0;\xi) = \boldsymbol{x}(t=0;\xi) = (1\,0)^T$, $\tau(t=0;\xi) = 0$ and $\tau(t;\xi) = 1$. For the reference dynamics, we choose the coefficient value $\overline{q} = q_0$. The set of ODEs is integrated using RK4 time with $\Delta t = 0.001$ for $t \in [0, 75]$.

We set $\alpha_0 = .01$ and $\alpha_1 = 0.2$, and use the same values previously selected for q_0 and q_1. Figure 2 shows trajectories of the solution $\boldsymbol{y}(t;\xi)$ in the state space for $t \in [0, 75]$, for the same realizations of $\xi(\omega)$ as previously selected, *i.e.*, $\xi(\omega) = 0$, ± 0.5 and ± 1. Plotted are results obtained with No = 5, which should be contrasted with the trajectories depicted in the first column of Figure 1. It is seen that unlike the Galerkin approximation of $\boldsymbol{x}$, the dynamics of $\boldsymbol{y}$ remain on the exact limit cycle and do not exhibit any spurious oscillation.

The results of Figure 2 demonstrate that the asynchronous time integration enables the simulation of the uncertain system over a long time period, whereas direct Galerkin projection of the governing equations would either fail or require a prohibitively large expansion order. In fact, the method is able to properly capture the trajectory of the system and its dependence with regard to some uncertain system parameter. However, this is achieved by expanding on the PC basis the system state at different physical times, such that the uncertain state $\boldsymbol{x}$ is not known at time t, but instead at random times $\tau(t;\xi)$. This raises the question of the type of statistical information on the dynamics that can be extracted from the asynchronous integration, or in other words from the computed $\boldsymbol{y}(t;\xi)$.

First, we verify that in addition to correctly capturing the trajectories in state space, the asynchronous integration also yields correct phase information. To this end, we plot in Figure 3 the solution component $\dot{y}(t;\xi)$ as a function of the rescaled time $\tau(t;\xi) \in [55, 60]$, and compare the resulting signal with the exact solution $\dot{x}(\tau;\xi)$ for the different realizations of $\xi(\omega)$. Figure 3 shows that, when it is properly expressed as a function of the uncertain clock, the numerical solution $\boldsymbol{y}$ indeed accurately approximates the exact solution. Specifically, for the present simple problem, the method allows us to track the system dynamics (uncertain phase and frequency) over arbitrary large integration times. It is also emphasized that repeating the same numerical experiment using a lower expansion order, No = 3, gives nearly identical results (not shown), and that predictions are weakly sensitive to the selected reference provided that $\overline{q} \in q_0 \pm q_1$.

To gain further insight in the effect of the time transformation, we plot in Figure 4 the evolution of the rescaled time for different realizations, as well as the evolution of the mean value $\langle \tau(y;\cdot) \rangle$ with 3 standard deviation bounds. Also plotted are curves of normalized values τ/t for different realizations $\xi(\omega)$. We observe that, as expected, τ is monotically increasing with t, and that the clock speed is larger for lower values of $\xi(\omega)$. Indeed, the system frequency decreases with decreasing $\xi(\omega)$, so the corresponding clock speed needs to be increased to catch up with the reference when $\xi(\omega) < 1/2$; conversely, the clock must be slowed down for $\xi(\omega) > 1/2$. It is also remarked that for $\xi(\omega) = 0$, we have $\tau(t;\xi(\omega)) \approx t$, since the reference is here defined by $\overline{q} = q(\xi(\omega) = 0)$. This can be better appreciated from the right plot in Figure 4. The curves of τ/t are limited to early times $t < 15$ since a constant asymptotic value is reached for longer times. Therefore, focusing on the initial stage of the dynamics, the normalized rescaled time τ/t first experiences fast adjustments over 2-3 periods of the system, before exhibiting damped oscillations toward its steady state. The characteristics of the early transient stage and damping rate depend on the parameters α_0 and α_1 of the asynchronous integration.

In fact, the asynchronous integration parameters have to be properly selected. The first parameter, α_0, has to be large enough to ensure a fast enough adjustment of the clock speed so as to prevent the emergence of the truncation errors that pollute the classical Galerkin solution (which corresponds to the case $\alpha_0 = 0$). However, if a very large α_0 is selected, the integration becomes unstable due to over adjustment. Similarly, the selection of α_1 is critical to control the asymptotic behavior of $\dot{\tau}$. The impact of the integration parameters on the resulting τ is illustrated in Figure 5, which depicts curves of $\tau(t)$ for different realizations of $\xi(\omega)$. Shown are results obtained for two different (α_0, α_1) pairs. Although varying (α_0, α_1) yields different rescaled times τ, it is emphasized that this does not significantly affect the results of the analysis of the uncertain system dynamics.

4.3. Uncertain period.

The first characteristic we wish to determine is the dependence of the period of limit cycle, $T(\xi)$, on the uncertain parameter $q(\xi)$. The period T^r of the reference system can be estimated from:

$$T^r = \lim_{t\to\infty} \frac{t}{N_c(t)}, \tag{46}$$

where $N_c(t)$ is the integer number of cycles completed by the reference system at time t. This quantity can be computed by counting the number of times the reference system crosses a prescribed plane intersecting the trajectory of $\boldsymbol{x}^r$. Since by virtue of the time rescaling, all realizations of the uncertain system remain essentially in phase with $\boldsymbol{x}^r$, $N_c(t)$ for large enough t is a correct indicator of the number of cycles completed for all values of the random coefficients q. Therefore, we can define the uncertain period as

$$T(\xi) = \lim_{t\to\infty} \frac{\tau(t;\xi)}{N_c(t)}. \tag{47}$$

This estimate of $T(\xi)$ at $t = 50$ is plotted in Figure 6 for a linear oscillator with $q_0 = (2\pi)^2$ and $q_1 = 0.3q_0$. The number of cycles N_c was incremented each time $\dot{x}^r$ changes of sign conditioned by $x^r(t) > 0$. Also indicated in Figure 6 is the exact period:

$$T(\xi) = \frac{2\pi}{\sqrt{q(\xi)}}.$$

Excellent agreement between the estimated and exact periods is observed.

4.4. Time-dependent statistics

Although we are primarily interested in the characterization of the limit cycle, we show in this subsection how time-dependent statistics can be retrieved from the asynchronous time integration. Let us assume that we want to compute the expectation of a functional $g : \mathbb{R}^n \mapsto \mathbb{R}$ of the state of the system $\boldsymbol{x}(t;\xi)$. Examples of such functionals are moments of $\boldsymbol{x}(t;\cdot)$.

The main difficulty here is that the uncertain state is not known at a specific time t, but at the rescaled time, *i.e.*, we have immediate access to $\boldsymbol{x}(\tau(t;\xi);\xi) = \boldsymbol{y}(t;\xi)$ only. Nevertheless, we still have all the information needed to reconstruct the expectation of $g(\boldsymbol{x}(t_a;\xi))$, at some selected time t_a. To this end, let us denote $\mathcal{S}$ a sample set of realizations $\xi(\omega)$ drawn at random from $p(\xi)$. Let m be the sample set size, and let $\xi^{(i)}$ be the i-th element of $\mathcal{S}$. For given time $t_a > 0$, and for each element of $\mathcal{S}$ we be denote $t^{(i)}$ the time such that

$$\tau(t^{(i)};\xi^{(i)}) = t_a, \quad i = 1,\dots,m. \tag{48}$$

We recall that $t^{(i)}$ is unique by virtue of the assumed properties of the rescaling. Then, the sample estimate of the expectation of $g(\boldsymbol{x}(t_a;\xi)$ can be expressed as:

$$\langle g(\boldsymbol{x}(t_a;\xi))\rangle \approx \frac{1}{m}\sum_{i=1}^{m} g(\boldsymbol{y}(t^{(i)};\xi^{(i)})). \tag{49}$$

In practice, $\boldsymbol{y}(t;\cdot)$ is known at discrete times so we rely on linear interpolations to approximate $\boldsymbol{y}(t^{(i)};\cdot)$.

To illustrate this approach, we evaluate the expectation $\langle x\rangle(t_a)$ of $x(t_a;\xi)$ and the standard deviation $\sigma(\dot{x})(t_a)$ of $\dot{x}(t_a;\boldsymbol{\xi})$, for the oscillator defined by $q(\xi) = (2\pi)^2(1+0.2\xi)$. For a fair comparison, we also compute reference values for $\sigma(x)(t_a)$ and $\langle x\rangle(t_a)$ through classical Monte Carlo sampling of the exact solution using a sample set with dimension $m = 50,000$.

Results are reported in Figure 7. The two plots of the top row compare the asynchronous time integration and Monte Carlo estimates of $\langle x\rangle(t_a)$ for t_a in the range $[0,15]$ and $[30,40]$ respectively. The asynchronous estimate uses the same sample set with dimension $m = 50,000$ as for the corresponding MC estimate. We observe that the two estimates are in excellent agreement for all the time intervals inspected. The plots of the second row of Figure 7 depict the same results but for the standard deviation of $\dot{x}$. Again excellent agreement is observed.

To better appreciate the accuracy of the computed moments, we present in the bottom of Figure 7 the error, defined as the absolute value of the difference between the instantaneous MC and asynchronous estimates, for different values of the sample set dimension, m. The results show that the error converges when the sample set dimension used to construct the asynchronous estimate increases. They also indicate that the error is essentially a function of m, and does not increase with t_a, as would be the case for a classical Galerkin projection, whose predictions at fixed expansion order deteriorate as time evolves.

Remark 5. *Some attention should naturally be given concerning the computational overheads involved in determining statistical moments of the solution, particularly contrasting levels corresponding to the classical Galerkin and asynchronous integration approaches. First, it is observed that for classical Galerkin integration, all realizations are computed at the same time t, which facilitates the computation of the desired moments. For instance, the variance of $\dot{x}(t_a;\xi)$ is immediately obtained from the PC expansion of the solution through:*

$$\sigma^2_{\dot{x}}(t_a) = \sum_{k=1}^{\mathrm{P}} \dot{x}^2_k(t_a). \tag{50}$$

However, if accurate moments are needed for large t_a, the required expansion order can be prohibitively large, as discussed previously. In contrast, the asynchronous time integration is much less demanding in terms of expansion order, and is not limited in terms of t_a. However, the determination of solution moments (or generally functionals) requires sampling, and the solution of (48) for each sample element. This amounts to the determination of the time t at which $\tau(t;\xi^{(i)})$ becomes greater than t_a; this is in turn achieved by

monitoring τ for each sample set element, through an efficient implementation where the functionals Ψ_k are computed once, and stored for each value $\xi^{(i)} \in \mathcal{S}$. As a result, the computational time simply scales with the sample set dimension m.

Remark 6. *The CPU cost of asynchronous integration should also be compared with the cost required by a classical Monte Carlo (MC) approach. Note that a MC simulation would achieve a similar level of accuracy, which is essentially governed by the sample set size m. Therefore, although the CPU load of MC also scales with m (for the time integration of m deterministic systems up to $t = t_a$), this ends up being much larger than that of the asynchronous time integration approach. This is the case because in the latter case, the problem reduces to integration of a single ODE system, whose size scales with* P.

5. Control formulation for asynchronous time integration

5.1. General framework

The general concept of the present methodology consists in designing a time transformation which acts so that the solution of the stochastic problem can be approximated using a low order expansion at all times. This amounts to determining the clock speed $\dot{\tau}$ so that the spreading of different realizations with respect to a reference remains small, and consequently that different realizations remain "in phase" with the reference realization. The time rescaling may then be assumed to be directly related to some quantity associated with the solution. In the previous section, a differential equation for $\dot{\tau}$ was suggested, and implemented as a hand-crafted 1st order ODE. As seen in the examples above, this approach is both intuitive, efficient and does not significantly increase the computational burden. However, in the case of a more complex system involving stiff dynamics, and possibly complex trajectories in the state space, such an approach may not be sufficiently efficient, and may even be ineffective due to the localized (in time) definition of the evolution of $\dot{\tau}$. One has then to resort to more robust strategies.

In this section, the time scaling $\dot{\tau}$ is determined using an optimization procedure. However, since it derives from the solution of an optimality equation based on a stochastic ODE, the approach may also suffer from the very same phenomenon it is supposed to cure. To avoid the need for an unacceptably large stochastic basis, $\dot{\tau}$ is determined over a prescribed, finite horizon, chosen so that a limited expansion is sufficient to derive an accurate solution. The minimization criterion may be imposed repeatedly over successive horizons and the derivation of the clock speed law $\dot{\tau}(t;\boldsymbol{\xi})$ then takes the form of a receding horizon optimization problem.

5.2. Control equations

The cost function associated with the optimization problem is described by a functional $\mathscr{J}$, which in its simplest form may be expressed as:

$$\mathscr{J} \equiv \frac{1}{2} \int_{T_c} \left(l_1 \, d^{2n_1} + l_2 \, e^{2n_2} \right) \, \| \boldsymbol{f}^r \| \, dt, \tag{51}$$

where $\{l_1, l_2, n_1, n_2\} \in (\mathbb{R}^+)^4$, the gap, Δ, is once again defined as:

$$\Delta(t;\boldsymbol{\xi}) \equiv (\boldsymbol{y} - \boldsymbol{x}^r) \cdot \boldsymbol{f}^r, \tag{52}$$

and the time drift rate, e, is defined according to:

$$e(t;\boldsymbol{\xi}) \equiv \dot{\tau}(t;\boldsymbol{\xi}) - 1. \tag{53}$$

The horizon, T_c, defines the time span over which the control is determined. Selection of the constants $\{l_1, l_2\}$ dictates how one wants to weight the different terms in the objective function. For instance, setting $l_1 \to +\infty$ will solely penalize the spreading of the realizations over the horizon T_c, whereas a large l_2 will prevent the clock speed from deviating too much from 1, and consequently act as a regularization term

aiming at ensuring $\dot{\tau} \geq 0$. The different terms of the cost are integrated along $\|\boldsymbol{f}^r\|\, dt$, *i.e.*, times where the reference has faster evolution are given larger weight. As seen above, the solution $\boldsymbol{y}$ of the rescaled dynamics obeys the governing equation:

$$\frac{d}{dt}\boldsymbol{y}(t;\boldsymbol{\xi}) = \dot{\tau}(t;\boldsymbol{\xi})\, \boldsymbol{f}(\boldsymbol{y};\boldsymbol{\xi}), \tag{54}$$

and so the problem can be formulated as: minimize the objective function $\mathscr{J}$ under the constraint that the governing equation is satisfied. This constrained optimization problem may be expressed using a Lagrangian, $\mathscr{L}$, defined as:

$$\begin{aligned} \mathscr{L} \quad \equiv \quad & \frac{1}{2}\int_{T_c} \left(l_1\, \Delta^{2n_1} + l_2\, e^{2n_2}\right)\, \|\boldsymbol{f}^r\|\, dt \\ & - \int_{T_c} \left(\frac{d\boldsymbol{y}}{dt} - \dot{\tau}\, \boldsymbol{f}\right) \cdot \boldsymbol{\lambda}\, \|\boldsymbol{f}^r\|\, dt, \end{aligned} \tag{55}$$

where $\boldsymbol{\lambda}(t;\boldsymbol{\xi}) \in \mathbb{R}^n$ is the adjoint variable.

One can show that minimizing $\mathscr{L}$ is equivalent to minimizing $\mathscr{J}$, and that the solution of the optimization problem satisfies the Lagrangian stationarity criteria:

$$\frac{\partial \mathscr{L}}{\partial \boldsymbol{\lambda}} = \frac{\partial \mathscr{L}}{\partial \boldsymbol{y}} = \frac{\partial \mathscr{L}}{\partial \dot{\tau}} = 0. \tag{56}$$

These conditions respectively yield:

$$\frac{d\boldsymbol{y}}{dt} - \dot{\tau}\, \boldsymbol{f} = 0, \qquad \text{State equation,} \tag{57}$$

$$\frac{d\boldsymbol{\lambda}}{dt} + \frac{\boldsymbol{\lambda}}{\|\boldsymbol{f}^r\|}\frac{d\|\boldsymbol{f}^r\|}{dt} + \dot{\tau}\, \boldsymbol{\nabla f}\, \boldsymbol{\lambda} + l_1\, n_1\, \Delta^{2n_1-1}\, \boldsymbol{f}^r = 0, \qquad \text{Adjoint equation,} \tag{58}$$

$$l_2\, n_2\, e^{2n_2-1} + \boldsymbol{f}\cdot\boldsymbol{\lambda} = 0. \qquad \text{Optimality equation.} \tag{59}$$

The "initial" condition for the adjoint variable is $\boldsymbol{\lambda}(t;\boldsymbol{\xi}) = 0$ at the time, t, corresponding to the end of the current horizon.

5.3. Solution method

A solution procedure to determine the optimal time rate may thus be described as follows: for a given guess initial $\dot{\tau}(\cdot;\boldsymbol{\xi})$ (for instance $\dot{\tau}(\cdot;\boldsymbol{\xi})$ of the previous horizon, or computed by means of the first-order method described in the previous sections):

1. solve the state equation (57) for $\boldsymbol{y}(t;\boldsymbol{\xi})$,
2. solve the adjoint problem (58) for $\boldsymbol{\lambda}(t;\boldsymbol{\xi})$,
3. solve (59) for $\dot{\tau}(t;\boldsymbol{\xi})$ using steepest descent / quasi-Newton algorithm,
4. go back to step 1 until convergence. In practice, the convergence is monitored by computing the residual of (59) at the end of step 2.

As with the previous approach, the successive resolutions of problems (57-59) are achieved through Galerkin projections of the corresponding ODEs and algebraic equation, relying on PC expansions of the stochastic quantities involved. The convergence is usually reached in a few iterations, typically less than 5-10, provided the objective function is indeed convex and the initial guess properly selected. As for all gradient-based methods, the above derivation only gives a local minimum but, provided the realizations of the trajectories are not too distorted compared to the reference one, the problem is likely to be convex, at least locally. Since the methodology proposed in his work is anyhow limited to such systems, the optimization step does not involve any pitfalls. Further, because the adjoint problem for $\boldsymbol{\lambda}$ is linear, it is inexpensive to solve, and the overall CPU cost is expected to be in line with that of the approach in section 3, and consequently to remain at a reasonable level.

6. Application to a nonlinear system

6.1. Formulation

In this section, we demonstrate the methodology presented above for a chemical system of the Belousov-Zhabotinsky (BZ) type. This kind of chemical system exhibits a sustained oscillation between two states due to an activator/inhibitor underlying mechanism. One of the simplest BZ-type models is the so-called Oregonator, [7, 6]. It basically describes the dynamics of a well-stirred, homogeneous system, governed by a three-species, coupled mechanism. The governing equations are given by:

$$\begin{cases} \dfrac{dX}{dt} = k_1\, Y(t) - k_2\, X(t)\, Y(t) + k_3\, X(t) - k_4\, X(t)^2, \\ \dfrac{dY}{dt} = -k_1\, Y(t) - k_2\, X(t)\, Y(t) + k_5\, Z(t), \\ \dfrac{dZ}{dt} = k_3\, X(t) - k_5\, Z(t), \end{cases} \tag{60}$$

where X, Y, and $Z \in \mathbb{R}^+$ denote the three species concentrations, and the coefficients $q = (k_1, \ldots, k_5)$ are reaction parameters. The initial conditions correspond to a deterministic mixture:

$$X(t=0) = Y(t=0) = Z(t=0) = 6000. \tag{61}$$

We are presently interested in the time evolution of the system state, defined as $\boldsymbol{x} = (X\ Y\ Z)^T$, in the case where the parameters are not accurately known. Specifically, some parameters are assumed uncertain and are modeled using statistically independent random variables lying in a given domain (see [12] for a discussion on the reaction rates modeling). To illustrate this scenario, k_1, k_2 and k_3 are taken to be deterministic and are given by:

$$k_1 = 2, \quad k_2 = 0.1, \quad k_3 = 104, \tag{62}$$

whereas k_4 and k_5 are considered to be uncertain, statistically independent, and respectively subjected to a 5% and 10% uncertainty levels, according to:

$$k_4(\omega) = 0.008\,(1 + 0.05\,\xi_1(\omega)), \tag{63}$$

$$k_5(\omega) = 26\,(1 + 0.1\,\xi_2(\omega)), \tag{64}$$

where $\boldsymbol{\xi} = (\xi_1, \xi_2)$ is uniformly distributed on $[-1, 1]^2$.

The left plot in Figure 8 shows a set of $m = 10$ deterministic trajectories obtained from the integration of (60) for randomly drawn realizations of the reaction constants $q(\boldsymbol{\xi}(\omega))$. The plot shows that for the range of system coefficients considered, the system converges asymptotically to a stable limit cycle. However, we observe that the asymptotic limit cycle depends on the reaction coefficients. The variability of the limit cycle with q also highly depends on the "phase" along the cycle, in other words on specific region of the state space. In particular, the trajectories are spread out at some locations, while they are clustered in the neighborhood of the origin.

We now apply the control-based approach detailed in section 5. The stochastic expansion basis consists of the two-dimensional (normalized) Legendre polynomials $\Psi_k(\boldsymbol{\xi}) = \Psi_k(\xi_1, \xi_2)$, which are truncated to second order, $\mathrm{No} = 2$. The dimension of the corresponding basis is $\mathrm{P} + 1 = 6$. The control parameters involved in the cost functional (51) are chosen as:

$$n_1 = 1, \quad n_2 = 1, \quad l_1 = 5 \times 10^{-13}, \quad l_2 = 5000, \tag{65}$$

For the integration of the ODEs (primal and dual problems) we again rely on a 4th order RK scheme, with fixed time step $\Delta t = 2 \times 10^{-4}$. The optimal control is carried out over the time horizon $T_c = 0.05$, corresponding to 250 time steps. For the reference dynamics, we select $\overline{q} = q(\boldsymbol{\xi}(\omega) = 0)$.

Controlled trajectories $\boldsymbol{y}(t;\boldsymbol{\xi}(\omega))$ are shown in the right plot of Figure 8. They correspond to the same realizations $\boldsymbol{\xi}(\omega)$ as used for the deterministic simulations shown in the left plot, thus allowing for a direct comparison. Excellent agreement between the corresponding predictions is observed, demonstrating the ability of the control strategy to provide a fine description of the limit cycle variability, even with a low expansion order (No = 2). It is important to note that if a straightforward Galerkin projection of the stochastic system is used, *i.e.*, without any time rescaling, a solution with No = 2 quickly diverges from the actual uncertain limit cycle, and exhibits non-physical features such as negative concentrations. For higher orders, the Galerkin computations may even become unstable (not shown) within a few periods of the system.

6.2. Time-dependent statistics

To assess quantitatively the efficiency of the asynchronous control scheme, we provide in Figure 9 a comparison between the the mean and variance of the first species concentration, $X(t;\boldsymbol{\xi})$, obtained using the control-based and Monte Carlo approaches. The Monte Carlo estimates use a sample set with dimension $m = 10^5$, whereas the control-based solution $\boldsymbol{y}$ is post-treated, as discussed in section 4.4, using a sample set also having $m = 10^5$. Thus, the sampling errors are of the same order for both methods. The plots show that the estimates for the two methods are in excellent agreement, as they are indistinguishable at the plot scale. In addition, it is emphasized that the error of the control-based prediction is not dependent on the observation time for the entire time span of the analysis; for the present example, this corresponds to roughly 41 periods of the reference system. Thus, arbitrarily large integration times may be selected, provided of course that time integration errors remain small.

We also observe that the signals depicted in Figure 9 involve two timescales. The fastest timescale corresponds roughly to the average period of the system along the uncertain limit cycles. The slowest timescale corresponds to the decay of the signal towards its asymptotic value: it is essentially governed by the rate of spread for the realizations along the uncertain limit cycle, and reflects the uncertainty in the period of the cycle induced by the uncertainty in the reaction parameters. Indeed, each realization completes a cycle within its own period $T(\omega)$, such that initially in phase realizations get more and more out of phase as time advances. Eventually, for large enough times, all realizations are totally out of phase and the two first moments reach their asymptotic equilibrium values.

6.3. Control of the realizations

The control-based method is specifically designed to counteract the spread of the realizations along their respective limit cycle, by determining an optimal time rescaling $\tau(t;\boldsymbol{\xi}(\omega))$ that maintains all realizations in a compact neighborhood. To illustrate this feature, we illustrate in Figure 10 the state of the system using selected (deterministic) realizations, and contrast these with predictions obtained using the for the case control-based approach at two different expansion orders No = 2 and 4. Results are generated at $t = 3.25$; this value is selected because it corresponds roughly to the phase of the reference dynamics at which the limit cycles experience their larger variability.

The left plot of Figure 10 shows that after only 4-5 periods of the dynamics, the uncontrolled realizations have spread out over nearly all the uncertain limit cycle. Also plotted are the 10 (randomly-selected) realizations of the limit cycle already shown in Figure 8. This is contrasted with the control-based approach (center and right plots), where all realizations of $\boldsymbol{y}(t = 3.25;\cdot)$ remain essentially contained in a cross section orthogonal to the reference trajectory, as expected from the optimization problem for $\dot{\tau}$. For the computations with No = 2, we remark that some realizations seem to fall far away from the the limit cycles. This is not due to an insufficient expansion order, but instead to an insufficient sampling of the uncertain limit cycle. To demonstrate this, we provide in the right plot results for No = 4 and 1,000 randomly-selected realizations of the limit cycle. It is seen that, at the scale of the plot, the distribution of $\boldsymbol{y}(t;\boldsymbol{\xi})$ is unaffected by increasing No; this is not surprising in light on the close agreement of the second-order and MC predictions of the first and second moments (Figure 9). The larger sample set of random realizations evidence that the uncertain limit cycle extends farther beyond the domain circumscribed by the 10 realizations shown in the center plot of Figure 10. Observations made at larger time (not shown) indicate that $\boldsymbol{x}(t;\cdot)$ continuously

spreads out, whereas $\boldsymbol{y}(t;\cdot)$ always remains on a compact region of the limit cycle. Another interesting observation is that the "boundary" of the limit cycle does not correspond to extreme values of $\boldsymbol{\xi}$, which reflects the nonlinear character of the system.

6.4. Rescaled time

To gain further insight on how the control maintains all realizations in a compact region of the state space, we present in the top plot of Figure 11 the evolution of the clock speed. The plot depicts the expected value $\langle\dot{\tau}(t;\boldsymbol{\xi})\rangle$ with $\pm$ one standard deviation bounds $\sigma(\dot{\tau})$. The evolution is reported for $t \in [33, 35]$, *i.e.*, over roughly 2.5 periods of the system; a non-periodic behavior is observed but with similar repeating patterns. The plot shows that the averaged clock speed remains close to $\dot{\tau} = 1$ at any time, with only small deviations limited to a few percent. The stability of the expected clock speed has to be contrasted with the evolution in time of its standard deviation. Over a period of the dynamics, the dynamics of the clock speed presents a characteristic pattern of alternated high and low (nearly zero) variability. A particularly noticeable feature is the presence of two successive peaks of high standard deviation, occurring over relative short time intervals of about 0.1, followed by longer periods of significant but lower variability which subsequently slowly decays to zero.

To understand this pattern, we plot in the bottom plot of Figure 11 the evolution of the species concentrations for the reference system. The figure shows that the clock speed experiences high variability when the reference system concentrations have the largest rates of change. This is expected because the clock speed is adjusted so as to maintain the realizations in some neighborhood, and because all realizations have similar dynamics but with different time scales. Clock speed adjustments are consequently critical when sharp evolutions occur, whereas in areas of the limit cycle where the state evolves slowly much weaker adjustments are needed. It is interesting to note that with the present value $T_c = 0.05$, roughly 16 successive horizons are needed to cover one period of the reference system. Thus, though it is computed independently over different time horizons, the control is able to adjust itself to the local conditions of the dynamics along the uncertain limit cycle. In particular, Figure 11 shows that the dynamics along the part of the cycle corresponding to low values of X and Z (bottom left part of the cycles in Figure 10) not only has a low variability in trajectory but also in phase velocity since virtually no control is needed along this segment of the cycle.

6.5. Probability density functions

To complete the analysis, we provide in Figure 12 the probability density function of the system period, and the asymptotic marginal distribution of the second species concentration $Y(t;\boldsymbol{\xi})$.

The uncertain period $T(\boldsymbol{\xi})$ is estimated from (46) after the reference system has completed $N_c = 45$ cycles. The density of $T(\boldsymbol{\xi})$ is in turn estimated by a sampling of $\boldsymbol{\xi}$ to construct histograms. The density has a trapezoidal structure, typical of the distribution of the sum of two independent random variables. However, the non-constant central part of the density denotes the combined interaction of the uncertain reaction coefficients k_4 and k_5 on the period.

For the marginal distribution of $Y(t;\boldsymbol{\xi})$, we select a time $t_a = 35$, large enough so the realizations are well spread along the uncertain limit cycle. We then sample $Y(t_a;\boldsymbol{\xi})$ to construct histograms approaching the density $p(Y)$, following the methodology used for the estimation of the statistical moments. We have also ascertained that the analysis time $t_a = 35$ was large enough to obtain the asymptotic distribution, namely by verifying close agreement, up to sampling errors, between the distributions computed at $t_a = 35$ and $t_a = 50$. We observe that the marginal density $p(Y)$ has a sharp peak around $Y \approx 400$, expressing again that the system spends a significant amount of time in this region where the variability induced by the uncertain inputs is the lowest.

7. Conclusions

This paper is concerned with quantifying the uncertainty associated with time-dependent physical systems involving random parameters. In case the system exhibits some level of periodicity, the straightforward

application of Galerkin PC methods is difficult, since the polynomial order required for accurate approximation of the solution increases with time, thus precluding long-term simulations. In particular, uncertain limit cycles and their associated statistics are generally difficult to determine using the classical approach. In addition, Monte-Carlo approaches may not always be feasible, particularly when the associated deterministic system is costly to simulate, leading to prohibitively large CPU times to obtain converged statistics.

To overcome the hurdles above, this paper explores the development of a computational approach based on a reformulation of the problem. The core concept amounts to the determination of an uncertain, time-dependent, time scale, selected so that the reformulated problem is essentially invariant in the "stochastically-stretched" time variable. In turn, this allows us to implement moderate-order PC expansions, namely without the need to continuously increase the truncation order.

Two strategies falling within the framework above have been developed. In both cases, we restrict our attention to simple systems which do not exhibit topological changes for the entire range of the random parameters. This restriction naturally excludes systems exhibiting chaotic dynamics or bifurcations, but on the other hand simplifies the testing of the resulting schemes.

The first strategy investigated relies on a heuristic linear time scaling. It basically consists in linearly adjusting the time scale of the uncertain system based on the phase difference measured with respect to a reference deterministic system. The resulting scheme is applied to an undamped linear oscillator with an uncertain frequency, and is shown to provide efficient and accurate predictions of the system uncertainty.

When the system limit-cycle involves more complicated dynamics, *e.g.*, with regions of low radius of curvature, a more sophisticated method for determining the stochastic time scale is necessary. To this end, an adjoint-based technique is developed, and applied to the example of a stiff chemical system with uncertain reaction rates. The adjoint-based approach is shown to provide accurate estimates with only a second-order PC expansion. While this second approach is a bit more demanding than the first from a computational standpoint, it is also more precise and, through the formulation of an associated cost functional, brings additional flexibility in the way by which the stochastic time scale is defined.

Future extensions of this work involve focusing on systems exhibiting more complex dynamics and higher dimensional limit-cycles. Potential avenues that we plan to explore include incorporation of the present approach with representations that enable us to capture steep variations or bifurcations. Such constructions are the subject of ongoing effort.

Acknowledgments

The work of OLM and LM is supported by the French National Agency for Research (ANR), Project ASRMEI JC08 #375619. LM also gratefully acknowledges the financial support of the Office of the Provost during his stay at Florida State University and the US NSF. The work of OMK is supported by the Department of Energy under Award Numbers DE-SC0002506 and DE-SC0001980. This report was prepared as an account of work sponsored in part by an agency of the United States Government. MYH was partially supported by the US NSF. Neither the United States Government nor any agency thereof, nor any of their employees, makes any warranty, express or implied, or assumes any legal liability or responsibility for the accuracy, completeness, or usefulness of any information, apparatus, product, or process disclosed, or represents that its use would not infringe privately owned rights. Reference herein to any specific commercial product, process, or service by trade name, trademark, manufacturer, or otherwise does not necessarily constitute or imply its endorsement, recommendation, or favoring by the United States Government or any agency thereof. The views and opinions of authors expressed herein do not necessarily state or reflect those of the United States Government or any agency thereof.

References

[1] M. Abramowitz and I.A. Stegun, "Handbook of mathematical functions," 9^{th} edition, Dover, New York, 1972.

[2] P. S. Beran, C. L. Pettit and D. R. Millman, *Uncertainty quantification of limit-cycle oscillations*, J. Comput. Phys., **217** (2006), 217–247.

[3] R. H. Cameron and W. T. Martin, *The orthogonal development of non-linear functionals in series of Fourier-Hermite functionals*, Ann. Math., **48** (1947), 385–392.
[4] M.K. Deb, I.M. Babuŝka and J.T. Oden, *Solution of stochastic partial differential equations using Galerkin finite element techniques*, Comp. Meth. App. Mech; Eng., **(190)**:(48) (2001), 6359–6372.
[5] B. Debusschere, H. Najm, P. Pébay, O. Knio, R. Ghanem and O. Le Maître, *Numerical challenges in the use of polynomial chaos representations for stochastic processes*, SIAM J. Sci. Comp., **(26)**:2 (2004), 698–719.
[6] I. R. Epstein and J. A. Pojman, "An introduction to nonlinear chemical dynamics: oscillations, waves, patterns, and chaos", Oxford University Press, New York, 1998.
[7] R. J. Field and R. M. Noyes, *Oscillations in Chemical Systems IV. Limit cycle behavior in a model of a real chemical reaction*, J. Chem. Phys., **60** (2004), 1877–1884.
[8] R. G. Ghanem and P. D. Spanos, "Stochastic finite elements: a spectral approach", Springer-Verlag, 1991.
[9] O. Le Maître, O. Knio, H. Najm and R. Ghanem, *Uncertainty qauntification using Wiener-Harr expansions*, J. Comput. Phys., **197**:1 (2004), 28–57.
[10] O.P. Le Maître, H.N. Najm, R.G. Ghanem and O.M. Knio, *Multi-resolution analysis of Wiener-type uncertainty propagation schemes*, J. Comput. Phys., **(197)**:2 (2004), 502–531.
[11] D. R. Millman, P. I. King and P. S. Beran, *Airfoil pitch-and-plunge bifurcation behavior with Fourier chaos expansions*, J. Aircraft, **42** (2005), 376–384.
[12] H. Najm, B. Debusschere, Y. Marzouk, S. Widmer and O. Le Maître, *Uncertainty quantification in chemical systems*, Int. J. Num. Meth. Eng., **80**:6 (2009), 789–814.
[13] C. L. Pettit and P. S. Beran, *Spectral and multiresolution Wiener expansions of oscillatory stochastic processes*, J. Sound Vib., **294** (2006), 752–779.
[14] X. Wan and G. E. Karniadakis, *An adaptive multi-element generalized polynomial chaos method for stochastic diffential equations*, J. Comput. Phys., **209** (2005), 617–642.
[15] N. Wiener, *The Homogeneous Chaos*, Amer. J. Math., **60** (1938), 897–936.
[16] J. A. S. Witteveen and H. Bijl, *An unsteady adaptive stochastic finite elements formulation for rigid-body fluid-structure interaction*, Comput. Struct., **86** (2008), 2123–2140.
[17] J. A. S. Witteveen and H. Bijl, *An alternative unsteady adaptive stochastic finite elements formulation based on interpolation at constant phase*, Comput. Methods Appl. Mech. Engrg., **198** (2008), 578–591.
[18] D. Xiu, I. G. Kevrekidis and R. G. Ghanem, *An equation-free multi-scale approach to uncertainty quantification*, Comput. Sci. Eng., **7** (2005), 16–23.
[19] D. Xiu and G.M. Karniadakis, *The Wiener-Askey Polynomial Chaos for stochastic differential equations*, SIAM J. Sci. Comput., **27** (2002), 619–644.

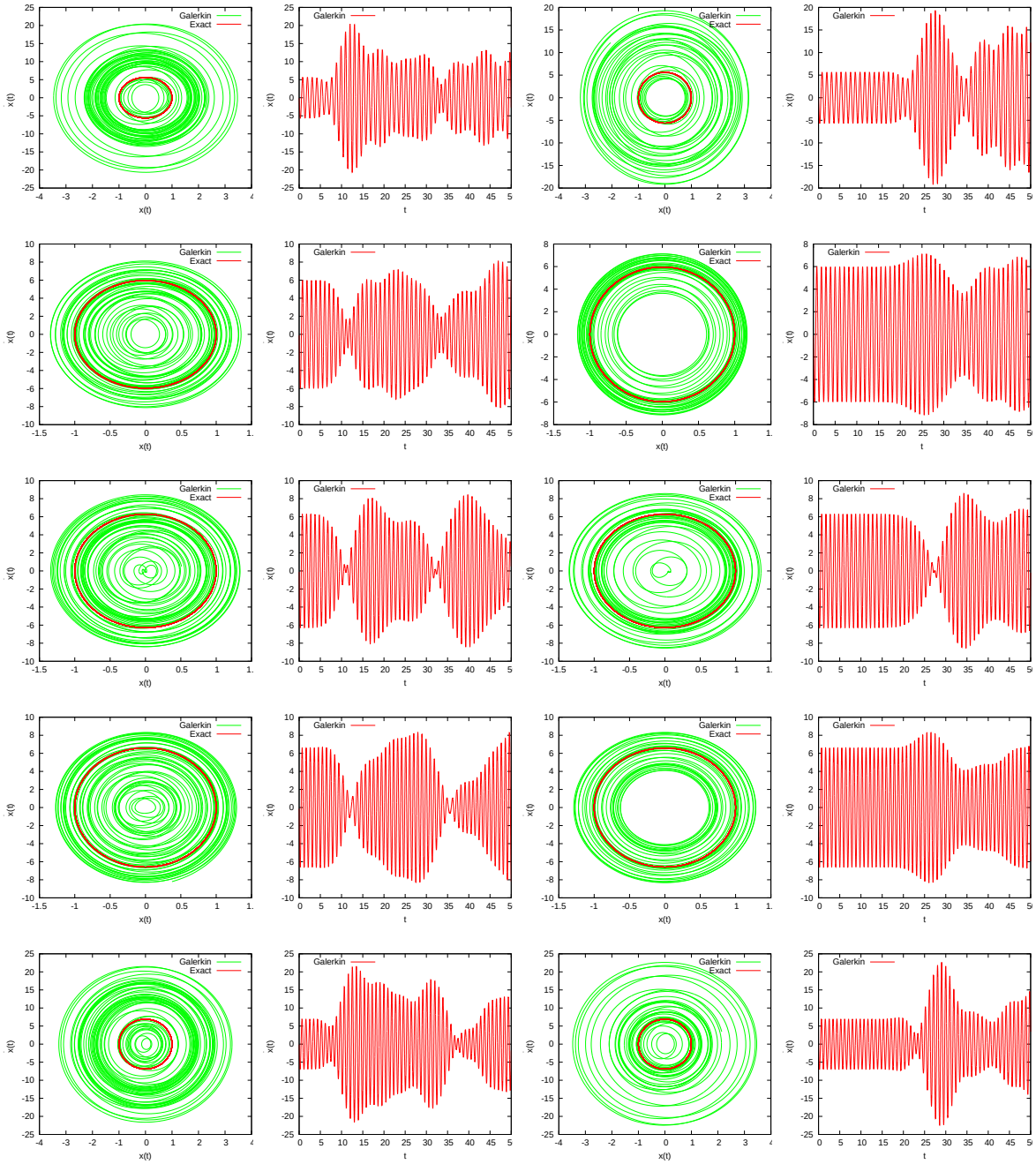

Figure 1: Trajectories in the state space of the classical Galerkin solution $\boldsymbol{x}(t;\xi)$ for No = 5 (first column) and No = 15 (third column), and predicted time evolutions of $\dot{x}(t;\xi)$ for No = 5 and 15 (second and forth columns, respectively). Trajectories and signals correspond to realizations $\xi(\omega) = -1$, $-1/2$, 0, $1/2$ and 1, respectively arranged from top to bottom.

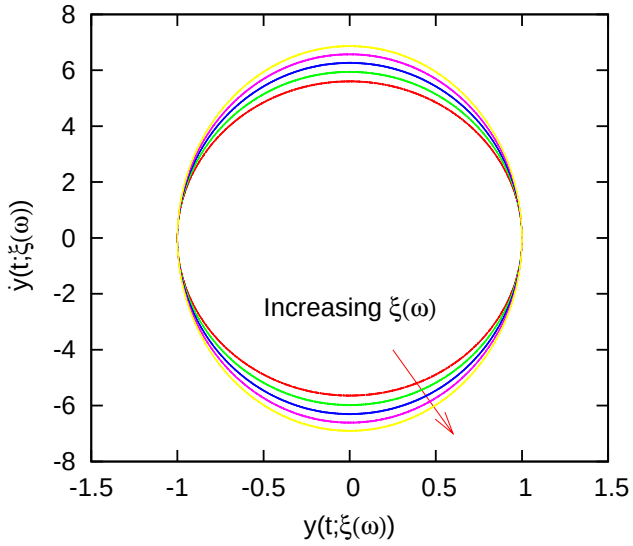

Figure 2: Trajectories of $\boldsymbol{y}(t;\xi)$ in the state space for $t \in [0, 75]$ and expansion order No = 5. Plotted are trajectories for realizations $\xi(\omega) = 0$, ± 0.5, and ± 1.

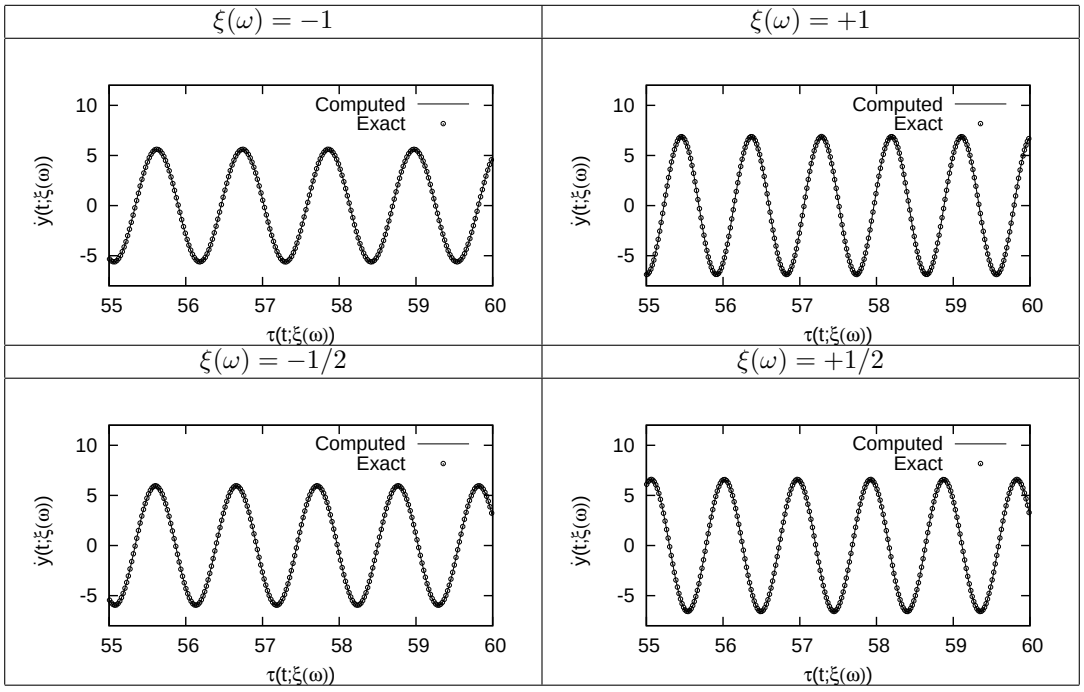

Figure 3: Evolutions of $\dot{y}(t;\xi(\omega))$ as a function of the rescaled time $\tau(t;\xi(\omega))$ (lines); the exact solution $\dot{x}(\tau;\xi(\omega))$ (symbol) is also shown for comparison. Plotted are curves corresponding to different realizations $\xi(\omega)$, as indicated. The computations are performed with No = 5.

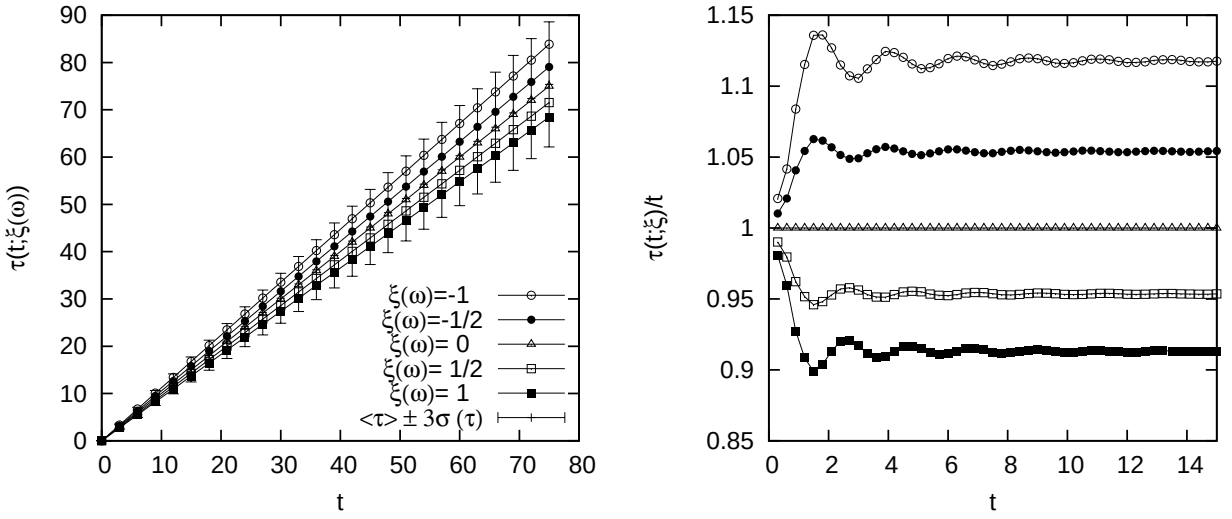

Figure 4: Left: evolution of the rescaled time $\tau(t;\xi(\omega))$ for different realizations of $\xi(\omega)$, as indicated. Also plotted is the expected rescaled time $\langle\tau(t;\cdot)\rangle$ with ± 3 standard deviation bounds. Right: evolution of the rescaled time τ normalized by t for the same realizations $\xi(\omega)$. Computations are performed with No $= 5$, $\alpha_0 = 0.01$, and $\alpha_1 = 0.2$.

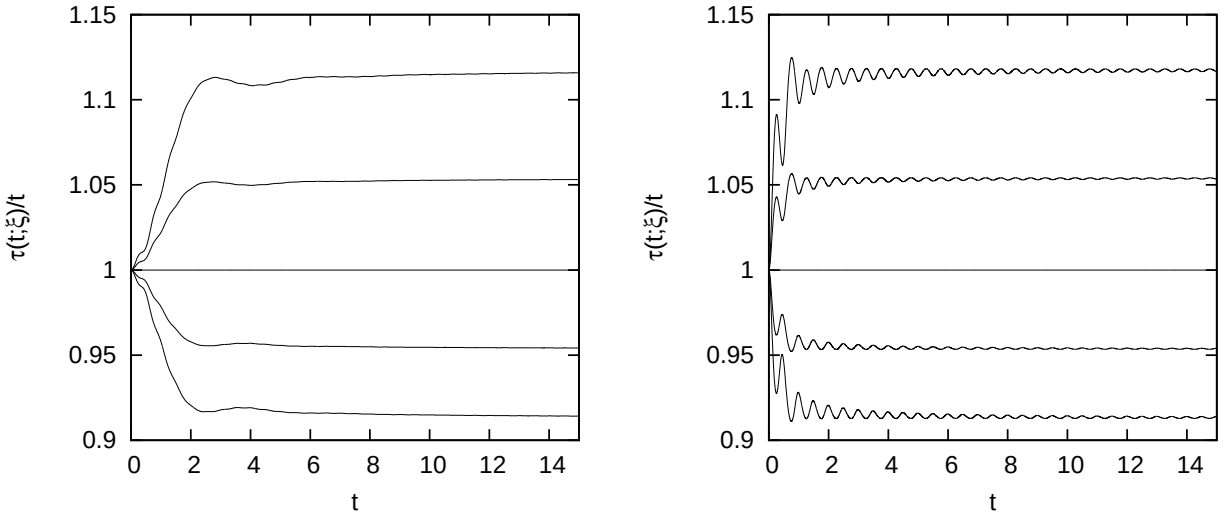

Figure 5: Rescaled time τ normalized by t for the same realizations $\xi(\omega)$ as in Figure 4; left: $\alpha_0 = 0.005$, and $\alpha_1 = 1$, right: $\alpha_0 = 1$ and $\alpha_1 = 10$. Computations are performed with No $= 5$.

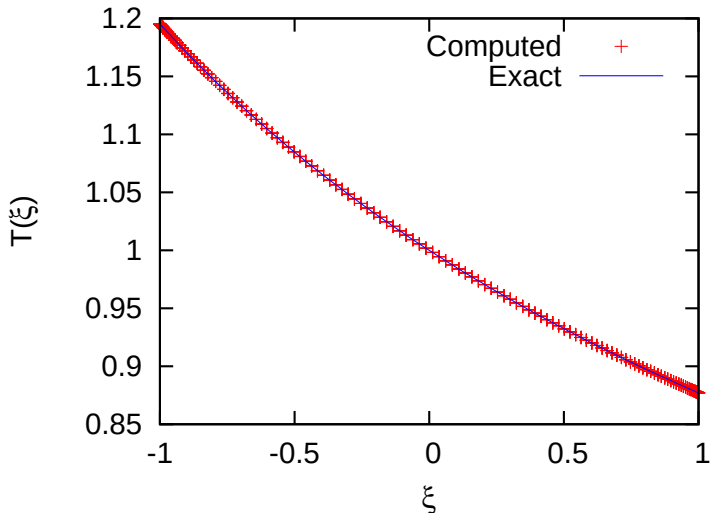

Figure 6: Computed and exact curves of $T(\xi)$ versus ξ, for the stochastic linear oscillator defined by $q(\xi) = (2\pi)^2(1 + 0.3\xi)$. Computations are performed with $\mathrm{No} = 5$

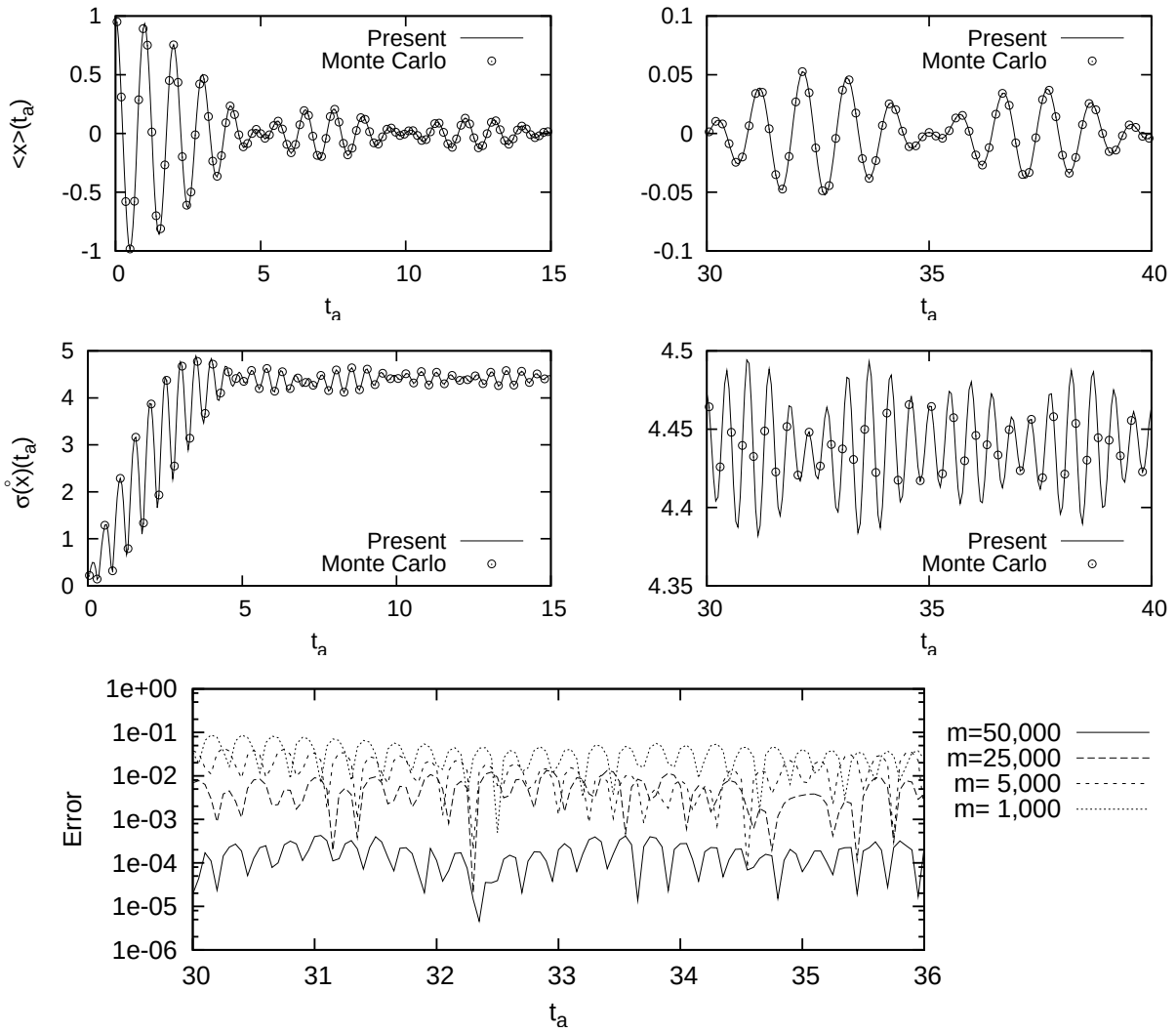

Figure 7: Top: estimates of $\langle x \rangle (t_a)$ for asynchronous and classical Monte Carlo sampling ($m = 50,000$). Middle: estimates of $\sigma(\dot{x})(t_a)$ for the asynchronous and classical Monte Carlo sampling ($m = 50,000$). Bottom: absolute value of the difference between asynchronous and Monte Carlo estimates of $\sigma(\dot{x})(t_a)$ for different sample sizes, m, as indicated. The asynchronous computation uses No $= 5$ and $\Delta t = 0.001$.

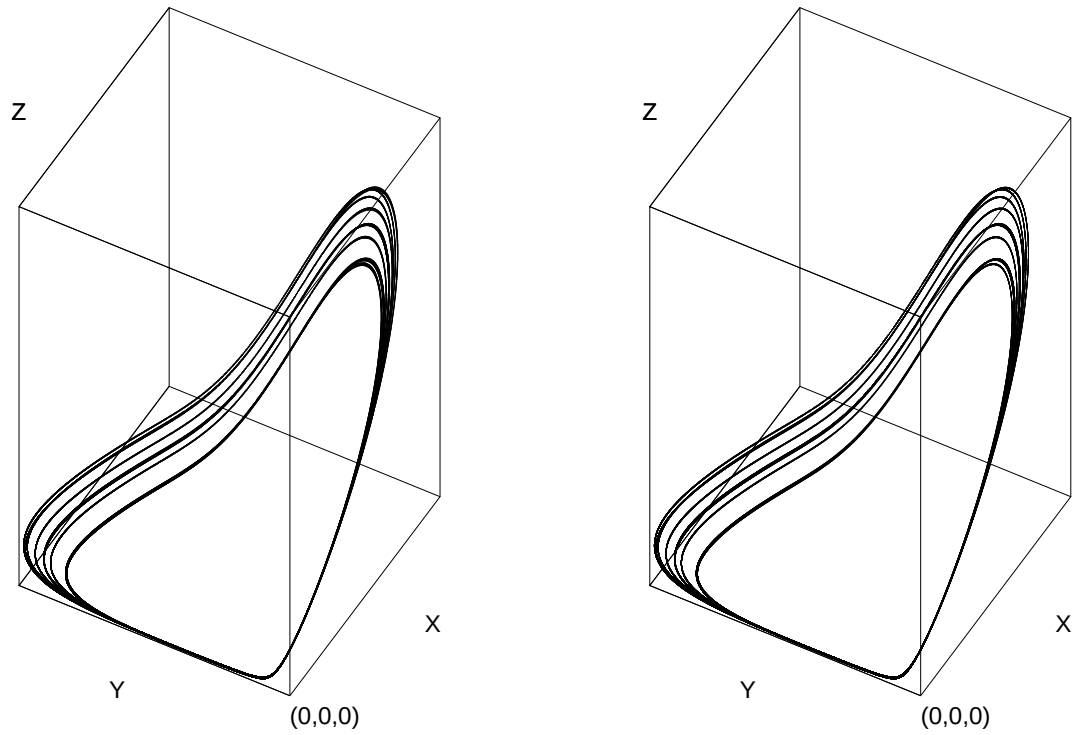

Figure 8: Trajectories in the state space of the uncertain chemical system. Left: deterministic simulations for 10 realizations of $q(\boldsymbol{\xi}(\omega))$. Right: reconstruction of controlled trajectories from the PC expansion of $\boldsymbol{y}(t;\boldsymbol{\xi})$ at No = 2 using the same realizations $\boldsymbol{\xi}(\omega)$ as in the left plot. In both cases, the trajectories are plotted for times $t \geq 5$.

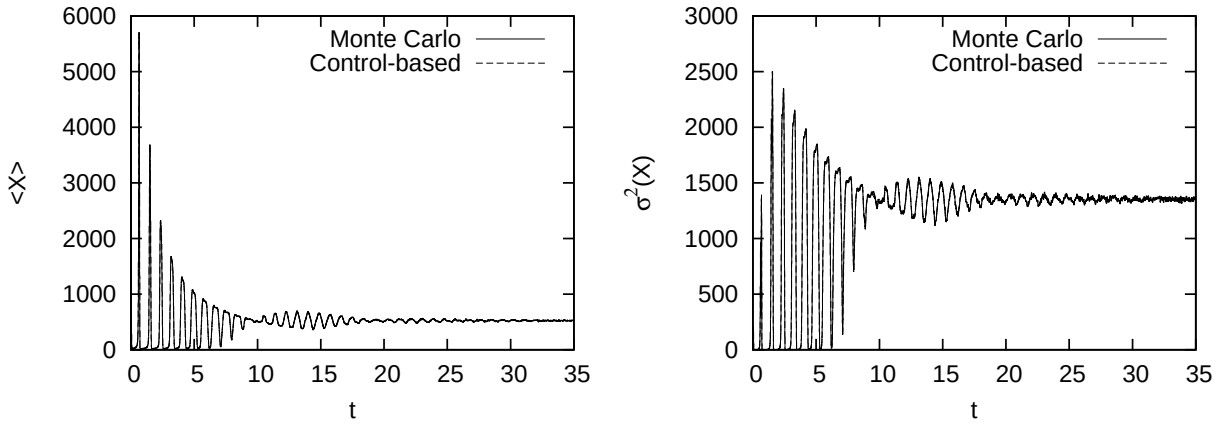

Figure 9: Comparison of Monte Carlo and control-based estimates of the mean value of the first specie concentration $\langle X \rangle (t)$ (left) and its variance $\sigma^2(X)(t)$ (right). The control-based computation uses No = 2 and the parameters given in (65).

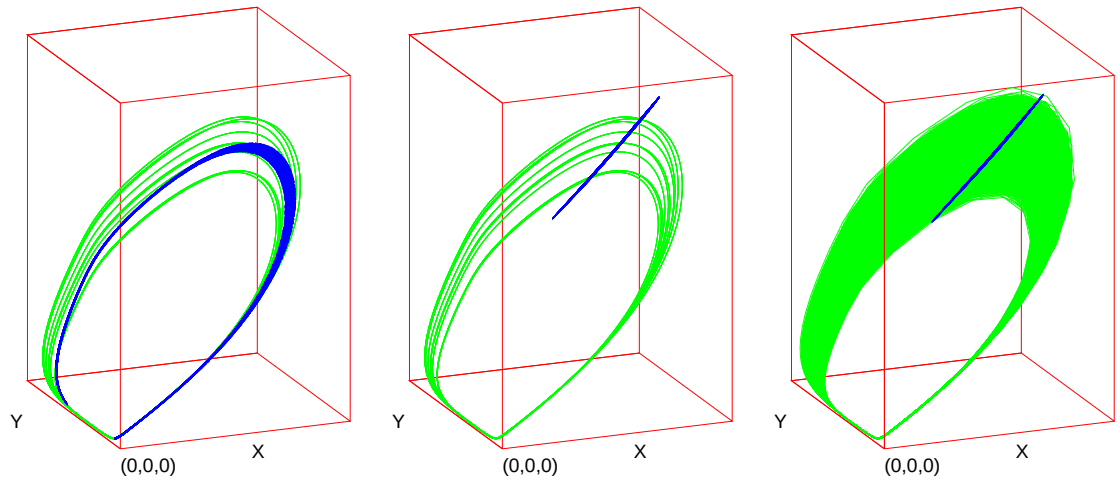

Figure 10: State of the uncertain system at $t = 3.25$ (blue dots) and sample set of the uncertain limit cycles (green lines). Left: realizations of the state $\boldsymbol{x}(t = 3.25; \boldsymbol{\xi})$ obtained by deterministic integration for 10 randomly-selected values $q(\boldsymbol{\xi}(\omega))$. Center: realizations of $\boldsymbol{y}(t = 3.25; \boldsymbol{\xi}(\omega))$ computed with the control-based strategy using No $= 2$ and $m = 10$ realizations of the limit cycle. Right: realizations of the rescaled state $\boldsymbol{y}(t = 3.25; \boldsymbol{\xi}(\omega))$ computed with the control-based strategy using No $= 4$ and $m = 1,000$ realizations of the limit cycle.

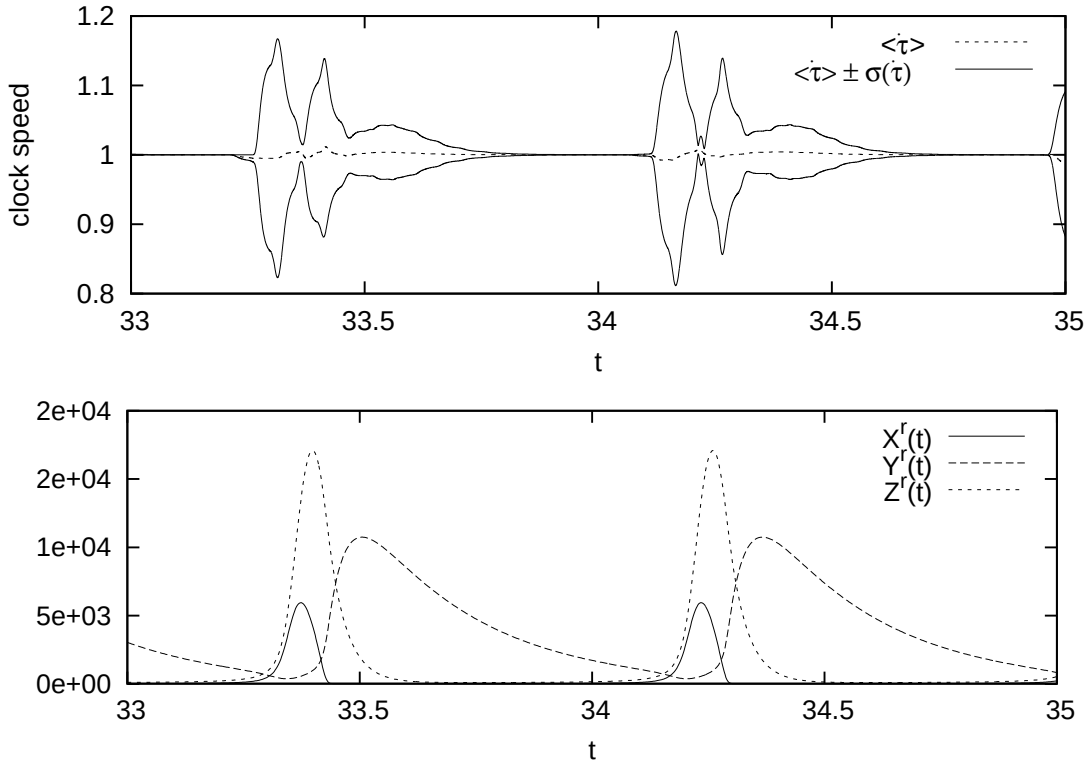

Figure 11: Top: evolution of the clock speed $\dot{\tau}$. Plotted are the expected clock speed with $\pm$ one standard deviation bounds. Bottom: evolution of the reference system concentrations.

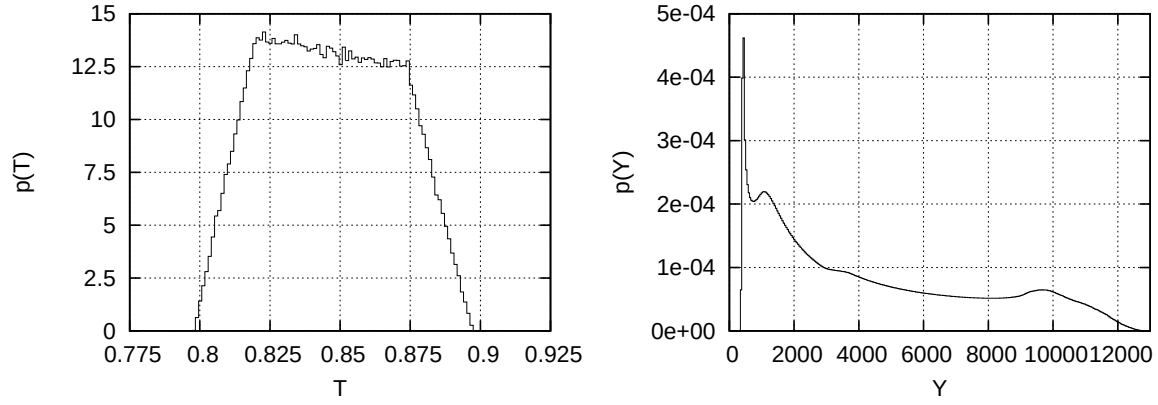

Figure 12: Left: probability density function of the system period. Right: asymptotic marginal distribution of the second species concentration.